Fabrication of Al matrix *in situ* composites via self-propagating synthesis

I. Gotman and M. J. Koczak

Department of Materials Engineering, Drexel University, Philadelphia, PA 19104 (USA)

E. Shtessel

Exotherm Corporation, Camden, NJ 08103 (USA)

Abstract

Al matrix composite materials with 30 vol.% TiC, TiB_2 and $TiC + TiB_2$ ceramic reinforcements were processed *in situ* via self-propagating high temperature synthesis (SHS) followed by high pressure consolidation to full density. Non-steady-state oscillatory motion of the combustion wave was observed during the SHS processing, resulting in a typical layered structure of the reaction products. The microstructure and phase composition of the materials obtained were studied using X-ray diffraction, optical microscopy and scanning (SEM) and transmission (TEM) electron microscopy. Very-fine-scale ceramic particles ranging from tens of nanometers up to 1–2 μm were obtained in the Al matrix. Microstructural analysis of the reaction products showed that the TiB_2/Al and $(TiB_2 + TiC)$/Al composites contained the Al_3Ti phase, indicating that full conversion of Ti had not been achieved. In the TiC/Al composite a certain amount of Al_4C_3 was detected. High room and elevated temperature mechanical properties (yield stress, microhardness) were obtained in the high-pressure-consolidated SHS-processed TiC/Al and TiB_2/Al composites, comparable with the best rapidly solidified Al-base alloys. These high properties were attributed to the high density of the nanoscale ceramic particles and matrix grain refinement.

1. Introduction

It is now widely recognized that aluminum-base metal matrix composites (MMCs) have a high potential for advanced structural applications when high specific strength and modulus as well as good wear resistance are important [1–5]. The properties of MMCs are controlled by the size and volume fraction of the reinforcement phase as well as by the microstructure and properties of the matrix–reinforcement interface: higher volume fractions of fine, thermally stable reinforcement yield higher mechanical properties of the composite. Traditionally, MMCs have been produced by such processing techniques as powder metallurgy, preform infiltration, spray deposition and various casting technologies, *e.g.* squeeze casting, rheocasting and compocasting [6–9]. In all the above techniques the reinforcement (usually in particulate form) is combined with the matrix material (either in molten or powder form). In this case the scale of the reinforcing phase is limited by the starting powder size, which is typically of the order of microns to tens of microns and

rarely below 1 μm. Studies of aluminum-base MMCs have been focused on the SiC/Al system mainly because of the availability and relatively low cost of SiC fibers, whiskers and particulates [7, 10, 11]. In spite of the rather high strength and modulus achieved, these composites have the problem of SiC–Al interaction at elevated temperatures, resulting in degradation of the matrix–reinforcement interface and deterioration of the mechanical properties.

In the last decade new *in situ* fabrication technologies for processing metal and ceramic composites have emerged. *In situ* techniques involve a chemical reaction resulting in the formation of a very fine, thermodynamically stable reinforcing ceramic phase during processing. Some of these technologies include DIMOX™, XD™, reactive gas infiltration and high temperature self-propagating synthesis (SHS) [6, 12–15]. Both TiC/Al and TiB_2/Al composites and composite powders with up to 40 vol.% of fine (1 μm or less) reinforcement were reported to have been successfully produced by the XD™ process [12, 16]. Infiltration of a carbonaceous gas in a molten Al–Ti

alloy was found suitable to form TiC/Al composites with a fine reinforcement size (0.1–3 μm) at low to moderate volume fractions (less than 15%) [14, 17].

SHS is an innovative processing technique which allows one to produce a wide range of refractory compounds from powder mixtures by utilizing the heat released during the exothermic reactions of their formation [18–21]. The ignition of a lightly compacted powder blend initiates a combustion wave that propagates through the blend, leaving behind the reaction products. The technique is extremely attractive, its main advantages being the self-generation of energy required for the process and the high productivity due to very high reaction rates. Originally employed for the production of single-phase ceramic compounds, SHS can be a feasible way for the in situ fabrication of composites, since both techniques utilize exothermic chemical reactions. The advantages of this processing route include submicron reinforcement size, nascent interfaces, economical processing, thermodynamic stability coupled with rapid reaction kinetics, and the ability to produce high volume fractions of ceramic reinforcements. Despite their intrinsic advantages, SHS-produced powders or porous bodies must be further processed to form dense materials. For SHS-processed MMCs, high pressure consolidation at room or slightly elevated temperatures (e.g. cold sintering) [22, 23] may become a feasible consolidation technique. In cold sintering, full-density net-shape parts are obtained by utilizing the plastic deformation of powders under high pressure. By this technique, compositions with up to 80 vol.% of hard particles can be consolidated to full density [24, 25].

Reports on in situ SHS processing of metal and intermetallic matrix composites (MMCs and IMCs) are scarce [15, 26–30]. In all these works except ref. 15, composites with very low fractions of matrix material (i.e. high fractions of reinforcing phases) were synthesized. In ref. 15, NiAl and FeAl matrix composites with 10–20 vol.% TiC, TiB$_2$, TiN and AlN particles were successfully fabricated by employing in situ SHS. In principle, SHS processing should be much more problematic for MMCs than it is for IMCs: for IMCs, both the reactions of the reinforcement and of the matrix formation are exothermic, whereas for MMCs the "inert" matrix acts as a diluent which may cause damping of the combustion wave. Therefore only ceramic reinforcements with high heats of formation are suitable for SHS processing of MMCs. Another basic requirement is the high fraction of ceramic reinforcement (i.e. low fraction of metal matrix). This ensures that the reaction will not be extinguished owing to excessive dilution by the matrix material. For Al-base MMCs, TiC and TiB$_2$ seem to be feasible reinforcements, both from the point of view of the

exothermicity of the reactions of their formation and from the point of view of their stability in Al. In ref. 30, TiC/Al composites were produced from a blend of Al and Ti powders and carbon fibers by employing SHS and subsequent consolidation with hot isostatic pressure (HIP). It was reported that at room temperature the self-propagating reaction front could not be sustained when more than 0.1 mole ratio of Al was added to the TiC mixture. Even with preheating of the starting mixture up to the melting point of Al, the authors did not succeed in fabricating composites with more than 0.3 mole ratio of the matrix phase (Al). The TiC/Al composite material obtained had a rather poor density (92%), even after the HIPing operation. In the present work, in situ SHS processing coupled with high pressure consolidation was successfully employed for the fabrication of dense Al-base MMCs reinforced with about 30 vol.% TiC, TiB$_2$ or TiC + TiB$_2$ particles.

2. Experimental procedure

2.1. Self-propagating synthesis

SHS processing of the Al matrix composites was performed by Exotherm Corporation, Camden, NJ. High purity (99.9%) titanium (less than 44 μm), aluminum (less than 44 μm) and boron (1–5 μm) from Atlantic Metals, carbon black (less than 0.2 μm, agglomerated) and boron carbide (B$_4$C, 1–7 μm) powders were used. Powder blends of compositions (in weight per cent) Al–34Ti–8.5C (1:1, Ti:C), Al–28.5Ti–12.9B (1:2, Ti:B), Al–30.6Ti–11.8B$_4$C (1:1, Ti:C; 1:2, Ti:B) and Al–30.6Ti–2.6C–9.2B (1:1, Ti:C; 1:2, Ti:B) were prepared by ball milling. Very small amounts (less than 1%) of halogenide-based gas transport agents were added to the starting powder mixture for the activation of the combustion process. Cylindrical compacts (32 mm diameter by 100 mm height) with about 36%–38% theoretical density were placed in a reactor with thermally insulated walls (Fig. 1). On top of each compact, 15 g of an igniting Ti–C mixture (1:1 mole ratio) were placed. The mixture was ignited by passing electric current through a tungsten wire. All SHS experiments were performed in argon at atmospheric pressure.

The temperature in the reaction zone was measured by two W–Re thermocouples placed a distance apart, the upper thermocouple being located at a distance of 40 mm from the igniting mixture (Fig. 1). Time of the wave front propagation between the two thermocouples was measured and the combustion wave velocity calculated. After the combustion, cylindrical samples with 30%–40% porosity were obtained.

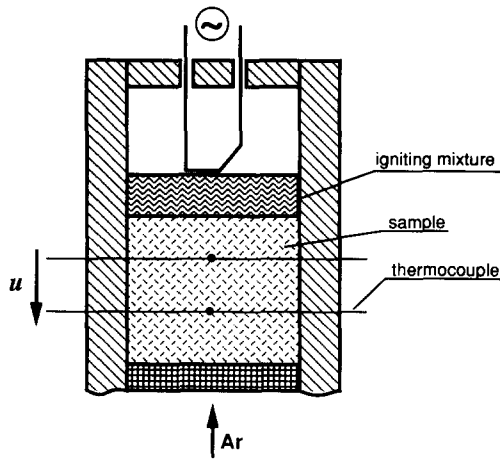The measured, calculated and estimated combustion parameters of the four different powder mixtures

Fig. 1. Schematic diagram of the SHS experiment.

(starting composition, final composition based on thermodynamic equilibrium, adiabatic temperature T_{ad}, combustion temperature T_{exp}, combustion wave velocity u and cooling time from T_{exp} to the freezing (melting) temperature of Al, t_{cool}) are listed in Table 1.

2.2. Consolidation, mechanical testing and microstructure characterization

For consolidation, two types of specimens were prepared:

(1) square specimens with cross-sections close to that of the high pressure cell (about $18 \times 18 \times 3$ mm^3) were cut from as-received porous material;

(2) as-received material was milled into powder (about 100 μm) which was subsequently compacted into approximately 70% dense green compacts.

Both types of specimens were treated in vacuum (about 10^{-5} Torr) at 300 °C for 1 h in order to remove the hydrate layer from the Al surface, then high pressure consolidated (cold sintered) at $P = 3$ GPa at room or slightly elevated (300 °C or less) temperatures. (It was previously reported that rapidly solidified Al alloy powders containing about 30 vol.% of fine intermetallic precipitates can be consolidated to full density by high pressure consolidation [31].) As a result of cold sintering, practically 100% density was achieved.

The microhardness of the as-received and cold-sintered materials was measured using a Vickers diamond pyramid under a load of 200 gf. For the cold-sintered materials the yield stress in compression σ_y, and the transverse rupture strength in three-point bending, σ_{TRS}, were measured. Specimens for mechanical testing (about $3 \times 3 \times 10$ mm^3 for compression and $3 \times 4.5 \times 18$ mm^3 for bending) were polished and annealed (500 °C, 1 h) prior to testing in order to minimize the possible strain-hardening effects caused by high pressure consolidation.

The phase composition of the SHS material was studied using X-ray diffraction (XRD). The material microstructure (polished samples, fracture surfaces) was investigated by optical microscopy, scanning electron microscopy (SEM) in secondary electron and backscattered electron modes, and transmission electron microscopy (TEM).

3. Results and discussion

3.1. Combustion synthesis

For all four compositions investigated, very low combustion velocities (at least one order of magnitude lower than those of pure TiC or TiB$_2$) were observed (Table 1). The propagation of the combustion wave was unstable, indicating that the rate of heat dissipation into the "inert" Al matrix was approaching the rate of heat generation. The non-steady-state oscillatory motion of the wave during combustion resulted in a typical layered structure of the reaction products. The heat required to maintain the propagation front of these reactions with the formation of 30 vol.% TiC and/or TiB$_2$, appears to be close to the lower limit required for the self-sustaining synthesis process.

3.2. Microstructure evaluation

XRD spectra of the as-received material after SHS for all four starting mixtures are presented in Figs. 2(a), 3 and 4. It can be seen that the phase compositions of the synthesized MMCs closely fit the predictions based on the thermodynamic equilibrium, *i.e.* the materials contain high fractions of TiC, TiB$_2$ and TiC + TiB$_2$ respectively. Representative micrographs demonstrating TiC and TiB$_2$ ceramic particles in the synthesized Al matrix composites are shown in Figs. 5–7. However, in all the systems except Al–Ti–C, strong additional peaks of Al$_3$Ti are observed, indicating that full conversion of Ti to TiC or TiC + TiB$_2$ has not been achieved. A representative micrograph of Al$_3$Ti needles in the Al–Ti–C–B system is shown in Fig. 8. It is assumed that, for all the compositions investigated, the combustion reactions are preceded by the melting of Al, followed by the capillary spreading of the molten Al along the solid Ti and carbon, boron or B$_4$C powder particles. This ensures intimate contact between Al and Ti, while there are only occasional points of contact between Ti and carbon, boron or B$_4$C. Upon heating, Al$_3$Ti is the first phase to be formed by a direct reaction between Ti particles and molten Al. The Al$_3$Ti formed is solid and remains solid throughout the combustion process (T_m of Al$_3$Ti (1340 °C) is higher than T_{exp}, see Table 1). According to the thermodynamic equilibrium, Al$_3$Ti should further react with carbon or boron to form the more

TABLE 1. Combustion parameters of the powder mixtures used

Starting powder mixture (wt.%)	Equilibrium combustion products (wt.%)	Volume fraction of ceramic particles	Adiabatic temperature T_{ad} (°C)	Combustion temperature T_{exp} (°C)	Combustion velocity u $(10^{-3}\,m\,s^{-1})$	t_{cool} (min)
Al 57.5 Ti 34.0 C 8.5	Al 57.4 TiC 42.45 Al$_4$C$_3$ 0.15	0.29	1128	1100	0.9	45
Al 58.6 Ti 28.5 B 12.9	Al 58.6 TiB$_2$ 41.4	0.30	1327	1260	1.9	54
Al 57.6 Ti 30.6 B$_4$C 11.8	Al 57.6 TiB$_2$ 29.6 TiC 12.8	TiB$_2$ 0.22 TiC 0.09	1176	1155	0.8	42
Al 57.6 Ti 30.6 B 9.2 C 2.6	Al 57.6 TiB$_2$ 29.6 TiC 12.8	TiB$_2$ 0.22 TiC 0.09	1297	1240	1.4	48

Fig. 3. X-Ray diffraction pattern of the SHS-processed TiB$_2$/Al composite.

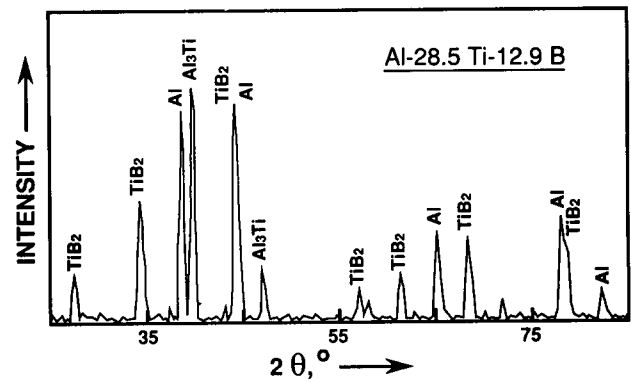Fig. 2. X-Ray diffraction patterns of the SHS-processed TiC/Al composite (a) as received and (b) after polishing.

thermodynamically stable TiC or TiB$_2$. The appreciable amounts of Al$_3$Ti phase in the final products (for Al–Ti–B, Al–Ti–B–C and Al–Ti–B$_4$C starting mixtures) show that, under the conditions of a propagating combustion wave, the dwell time of the material in the combustion zone is not long enough to achieve the equilibrium compositions. An interesting observation is that the relative intensities of the Al$_3$Ti X-ray peaks do not match the standard intensities and differ from spectrum to spectrum. A possible explanation, suggested by the layered structure of the SHS reaction products, is that the Al$_3$Ti needles have a certain preferred orientation with respect to the direction of the combustion wave propagation. Since Ti is partly converted to Al$_3$Ti instead of the expected TiC or TiB$_2$, some of the carbon, boron or B$_4$C should either remain unreacted or form carbides or borides other than TiC and TiB$_2$. However, no peaks of Al carbide, Al borides or B-rich Ti borides were detected in the X-ray spectra of the as-received TiB$_2$/Al and (TiB$_2$ + TiC)/Al materials. The unreacted amorphous
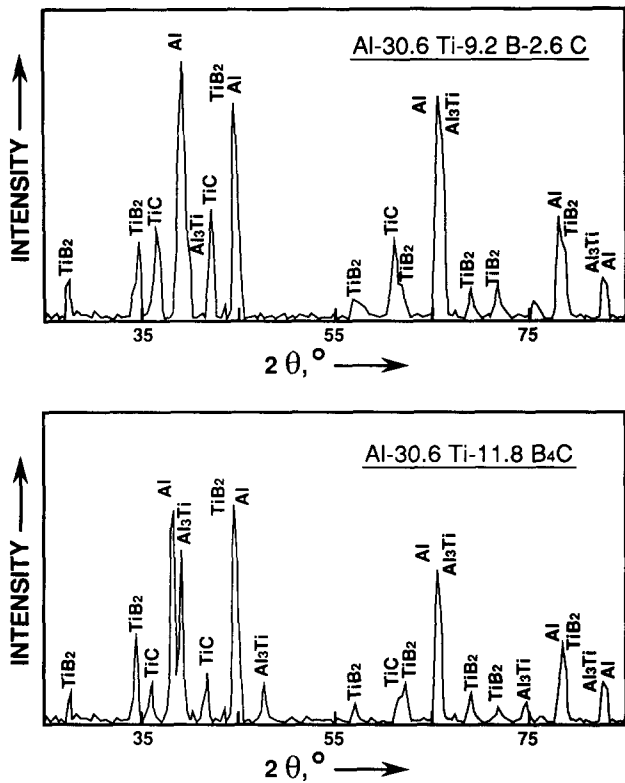
Fig. 4. X-Ray diffraction patterns of the $(TiC + TiB_2)/Al$ composites SHS processed from (a) Al–Ti–B–C starting mixture and (b) Al–Ti–B_4C starting mixture.
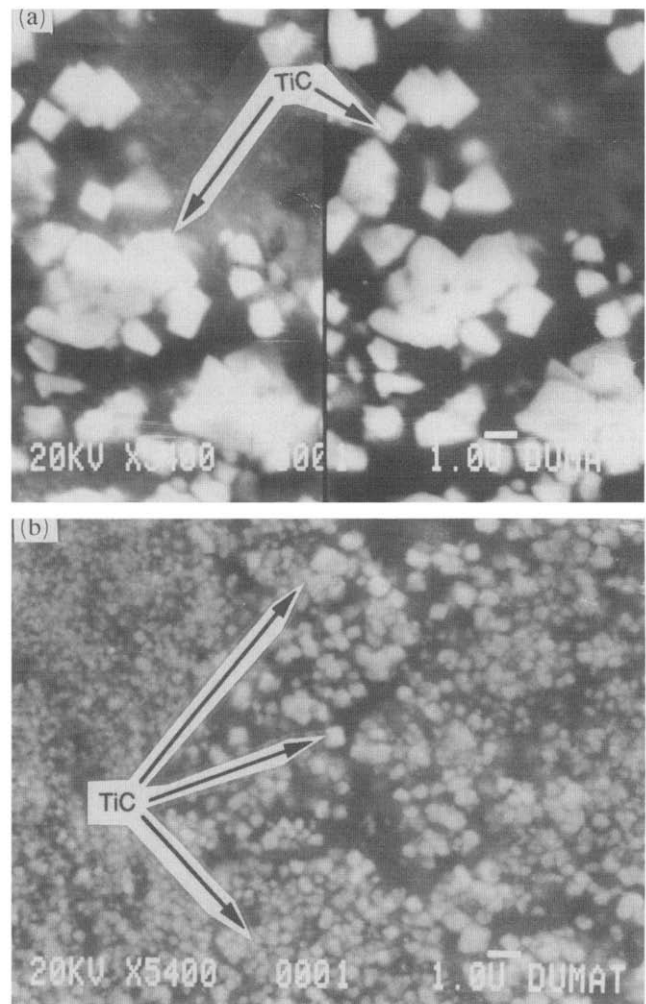

Fig. 5. Representative microstructures (SEM) of the TiC/Al *in situ* composite (as received after SHS): (a) relatively coarse TiC particles, left—secondary electron image, right—backscattered electron image; (b) fine TiC particles.
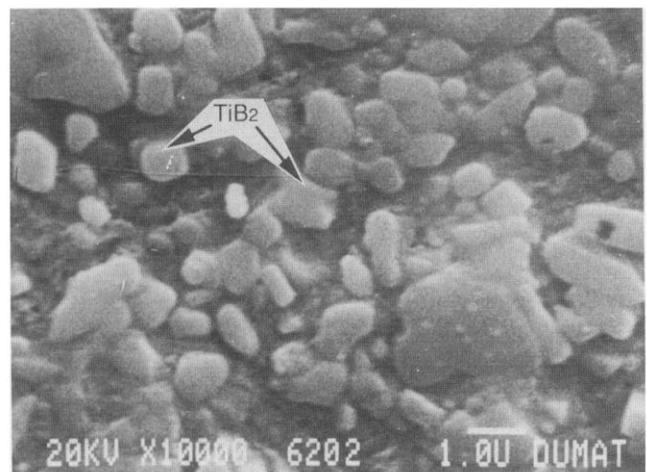
carbon or boron, if present, will not give detectable peaks in X-ray diffraction spectra; X-rays are also insensitive to small amounts of B_4C.

The X-ray spectrum of the as-received material after SHS of the Al–Ti–C starting mixture (Fig. 2(a)) shows that for this composition there is practically no Al_3Ti phase in the final product. However, the micrographs in Figs. 9(a) and 9(b) reveal the presence of some needle-like formations resembling Al_3Ti. There is no contrast difference between these needles and the matrix in the backscattered electron image, suggesting that their composition is similar to that of the matrix. According to the wavelength-dispersive X-ray (WDX) map in Fig. 9(c), the needles, as well as the matrix, contain both Ti and Al, whereas the darker phase surrounding the needles contains only Al. Since the only two phases detected in the polished Al–Ti–C sample are Al and TiC (Fig. 2(b)), the dark phase must be pure Al and the brighter phase (both the needles and the matrix) a very fine mixture of Al and TiC. In our opinion the needles in the final microstruture indicate that a transient Al_3Ti phase was present in the course of the SHS processing. It is possible that, similarly to the previous compositions, the SHS process in the Al–Ti–C starts with the formation of Al_3Ti. These

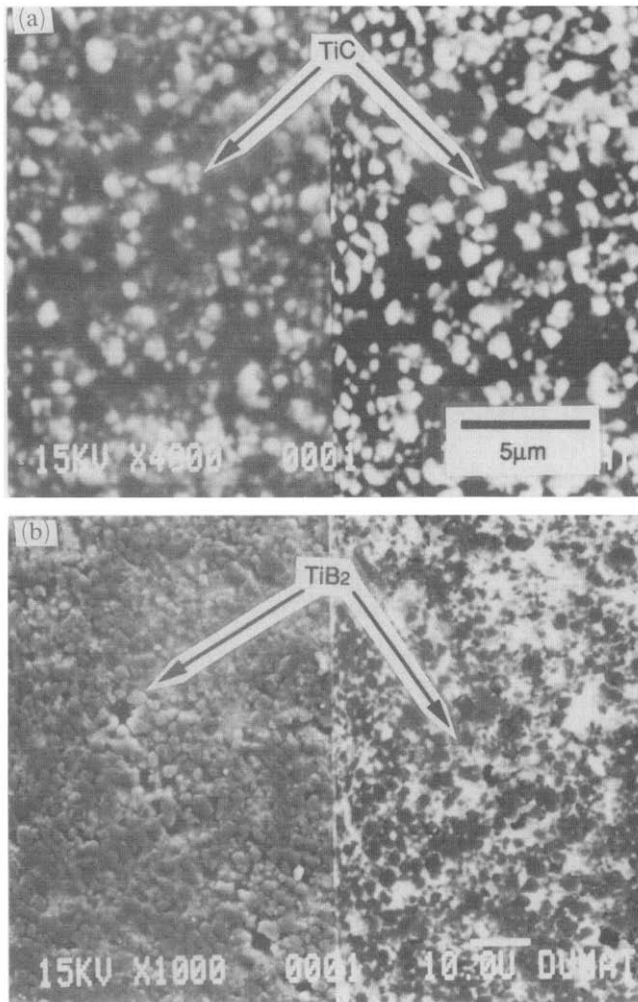Fig. 6. Representative microstructure (SEM) of the SHS-processed TiB_2/Al *in situ* composite (cold sintered).

Fig. 7. Representative microstructures (SEM) of the $(TiC + TiB_2)/Al$ *in situ* composite (as received after SHS of Al–Ti–C–B mixture): (a) TiC particles; (b) TiB_2 particles, left—secondary electron image, right—backscattered electron image.

Fig. 8. Al_3Ti needles in the microstructure of the $(TiC + TiB_2)/$ Al composite SHS processed from Al–Ti–C–B mixture: (a) optical micrograph; (b) SEM image, left—secondary electron image, right—backscattered electron image.

Al_3Ti needles further react with carbon to form Ti_2AlC ternary carbide (H phase), finally decomposing into fine-scale precipitates of TiC (*e.g.* $Ti_2AlC + C = Al + 2TiC$). Thus no Al_3Ti phase is present in the final product. Such a reaction path would be in agreement with the ternary Al–Ti–C system phase equilibria [32]. A similar sequence of events leading to the formation of TiC reinforcements in aluminum was suggested in refs. 17 and 33. This mechanism, however, accounts only for the formation of a relatively small amount of secondary TiC.

It is assumed that solid state reactions at the Ti–carbon or Ti–boron powder particle interfaces, as well as surface reactions between carbon or boron particles and Ti dissolved in the molten Al, are important mechanisms of ceramic reinforcement formation during the SHS processing. These reactions should yield rela-
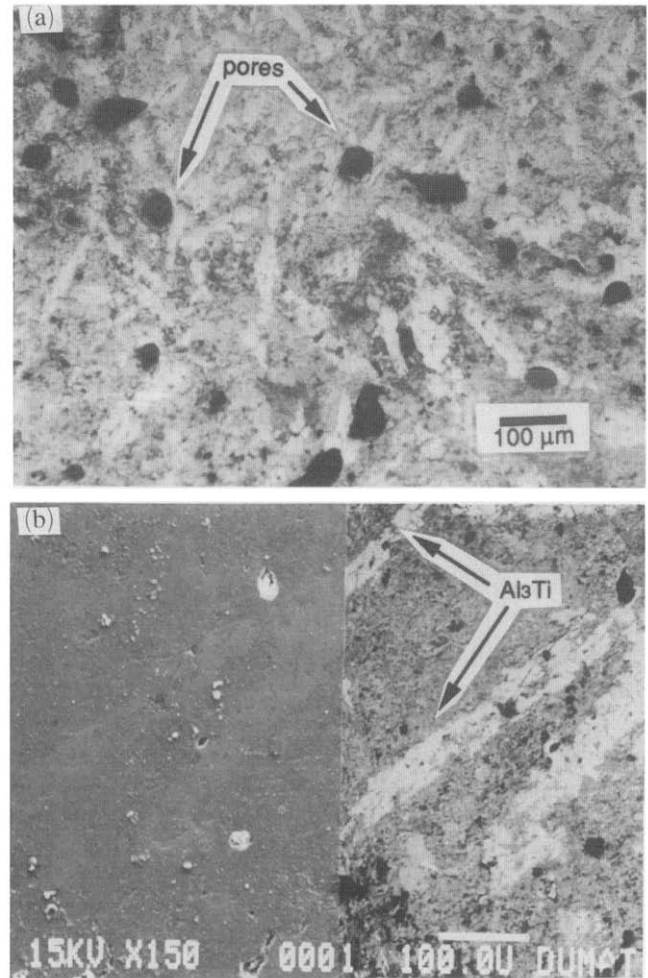
tively coarse TiC and TiB_2 particles comparable in size with the starting powder particles. Indeed, 1–2 μm size TiC and TiB_2 dispersions can be clearly seen in the SEM images in Figs. 5(a), 6 and 7. However, the micrograph in Fig. 5(b) reveals the existence of the whole population of considerably finer-scale (about 0.1 μm) TiC particles. Very fine TiC and TiB_2 particles can also be seen on the fracture surfaces of TiC/Al and TiB_2/Al composites (Fig. 10). The TEM image in Fig. 11 bears evidence of the very fine microstructure of the TiC/Al material obtained: grains as fine as 30 nm are clearly seen, though it is difficult to distinguish between different phases owing to the high volume fraction of the fine TiC dispersions. Their size, shape and homogeneous distribution suggest that these TiC particles were not formed by an interfacial reaction but rather by precipitation from the solution. Though very fine TiB_2 par-
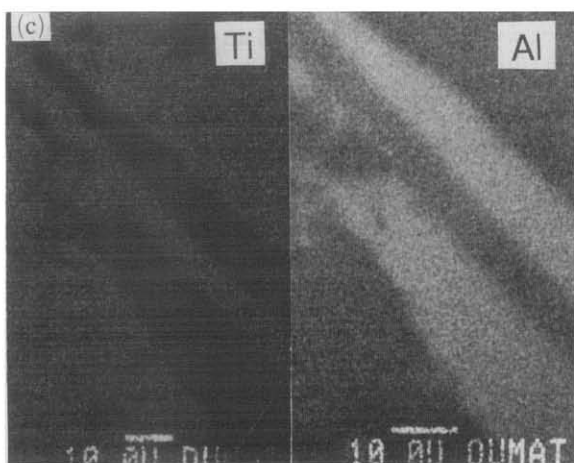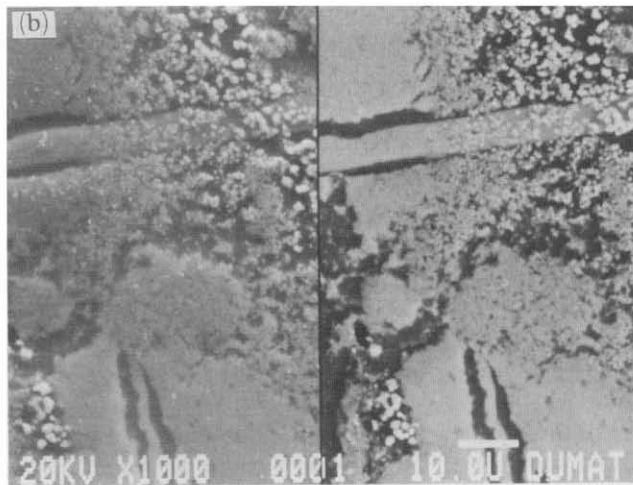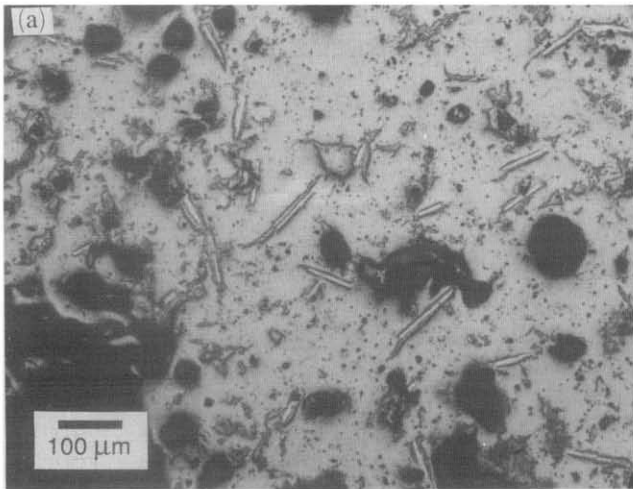
Fig. 9. Al$_3$Ti-like needles in the microstructure of the SHS-processed TiC/Al *in situ* composite: (a) optical micrograph; (b) SEM image, left—secondary electron image, right—backscattered electron image; (c) Al and Ti WDX maps of the needle and surrounding area.
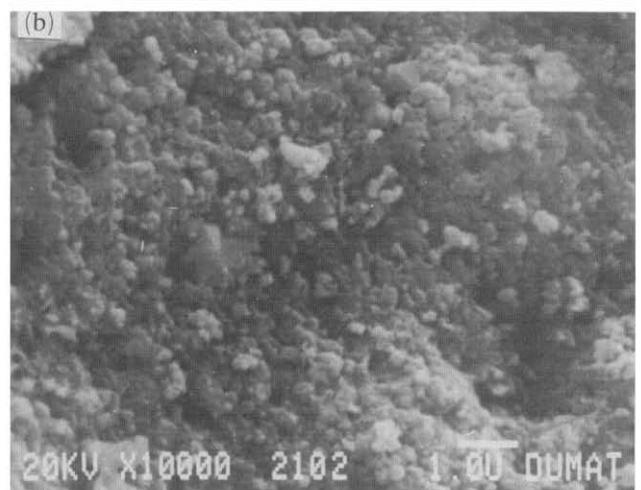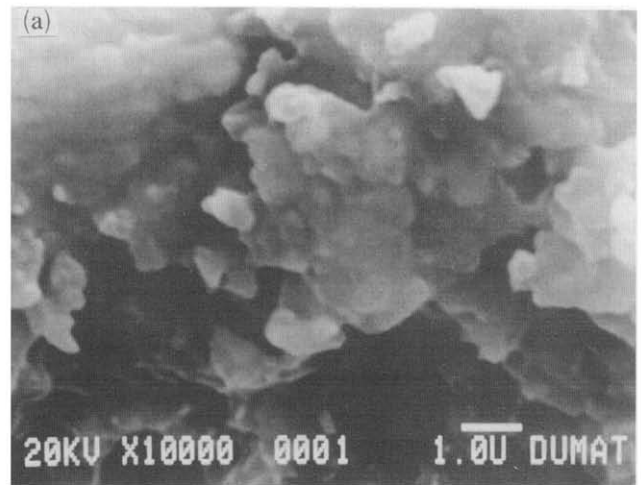

Fig. 10. Fracture surfaces in bending (SEM) of the SHS-processed *in situ* composites (a) TiB$_2$/Al, (b) and (c) TiC/Al.

ticles are not seen as clearly as TiC particles, their existence will be further confirmed by the high mechanical properties of the TiB$_2$/Al composite. As a matter of fact, TiB$_2$ particles are more likely to be
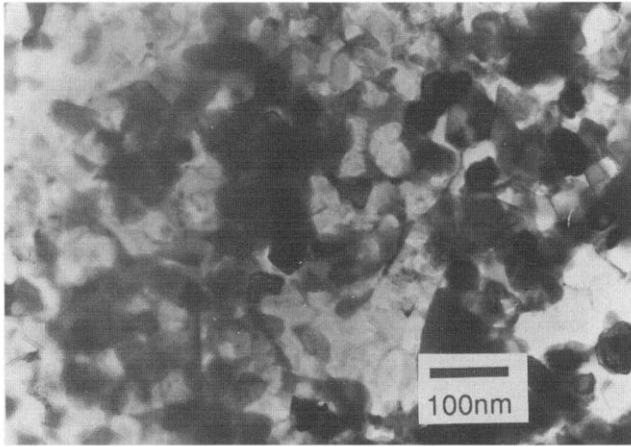
Fig. 11. TEM image of the SHS-processed TiC/Al *in situ* composite.

formed by the solution–reprecipitation mechanism than are TiC particles. Since the concentrations of boron and Ti in molten Al at 1260 °C (T_{exp} for TiB$_2$/Al composite processing) can be as high as about 1.7 and 17 wt.% respectively [34], the reaction between dissolved Ti and B atoms with precipitation of solid TiB$_2$ (T_m of TiB$_2$ (2790 °C) is much higher than T_{exp}) is highly probable. At the same time the solubility of carbon in liquid Al at 1100 °C (T_{exp} for TiC/Al composite processing) is very limited (800 p.p.m. as extrapolated from ref. 35, or even 45 p.p.m. [36]), making precipitation of TiC from the melt much less likely. Clearly the mechanism of formation of nanoscale TiC particles during the SHS processing of Al matrix composites requires further investigation.

In the case of the Al–Ti–C system, relatively large (less than 0.5 mm) "islands" of unreacted carbon black are visually observed in the specimens after the SHS treatment. The presence of unreacted carbon implies that the ball-milling operation was not effective in disintegrating and distributing the agglomerates of the otherwise fine starting carbon black powder. Under the conditions of the rapidly propagating combustion wave, there is not enough time for the relatively coarse carbon agglomerates either to dissolve or to be fully consumed by interfacial reaction with the surrounding metal. Since the ratio of carbon to Ti in the starting mixture was 1:1 (by moles), some unreacted Ti is expected to be found in the final material. However, no peaks of Ti metal are detected in the X-ray spectrum (Fig. 1). It is possible taht in this case the TiC is slightly hyperstoichiometric (TiC has an extremely wide range of homogeneity). It is evident from the X-ray spectrum that the amount of Al$_4$C$_3$ in the as-received TiC/Al material after SHS is well above the expected 0.15 wt.%. This aluminum carbide may have been formed

either by a direct reaction between carbon and the molten Al or by the reaction of TiC with the Al melt during cooling after the combusion. Indeed, Al$_4$C$_3$ was reported to be formed on TiC in Al–Ti liquids containing carbon at temperatures below 1273 K [37]. It was assumed that Al$_4$C$_3$ is formed by the following reaction: $3TiC + 13Al_{(liq)} = Al_4C_3 + 3Al_3Ti$ [38]. In our case the cooling time from the combustion temperature (1373 K) to T_m of Al is relatively long (45 min) and may be sufficient for an appreciable amount of Al$_4$C$_3$ to be formed. If the formation of Al$_4$C$_3$ at temperatures below 1273 K is of the equilibrium origin, as it is claimed in ref. 38, one cannot expect to fabricate, by SHS processing, Al$_4$C$_3$-free TiC/Al composites owing to the conversion of TiC to Al$_4$C$_3$. It should be mentioned that determining the exact location of the Al$_4$C$_3$ phase by studying the SHS-processed TiC/Al composite by optical microscopy or SEM could be helpful in establishing whether Al$_4$C$_3$ is formed by the direct reaction between Al and carbon or at the TiC–Al interface during cooling. Unfortunately though, Al$_4$C$_3$, being a hygroscopic compound, was completely dissolved in water used during the preparation of the metallographic samples. (The X-ray spectrum of the polished samples contains no peaks of Al$_4$C$_3$, see Fig. 2(b).)

3.3. Mechanical properties

The results of the mechanical testing of the cold-sintered SHS-processed Al matrix composites are encouraging. (No difference in the mechanical properties was observed for samples consolidated from pulverized or directly from as-received materials after SHS.) In the bending test relatively high values of σ_{TRS}, *i.e.* 550 and 740 MPa for TiC/Al and TiB$_2$/Al composites respectively, were obtained. The results of the compression test at various temperatures for the cold-sintered TiC/Al and TiB$_2$/Al materials are presented in Fig. 12. High values of the yield stress σ_y have been obtained for both compositions ($\sigma_y = 430$ and 560 MPa at room temperature for TiC/Al and TiB$_2$/Al composites respectively). For the TiB$_2$/Al composite the dependence of σ_y on temperature is similar to the tensile strength behavior of materials fabricated from rapidly solidified aluminum alloy powders with a similar volume fraction (about 30%) of intermetallic phases [39]. Correspondingly high Vickers microhardness numbers (VHNs) were achieved: VHN = 225 ± 5 for TiC/Al and VHN = 245 ± 5 for TiB$_2$/Al composite.

A wide range of controversial viewpoints are currently available on the strengthening of metal matrix composites. Various workers have proposed that the mechanical behavior of MMCs can be understood
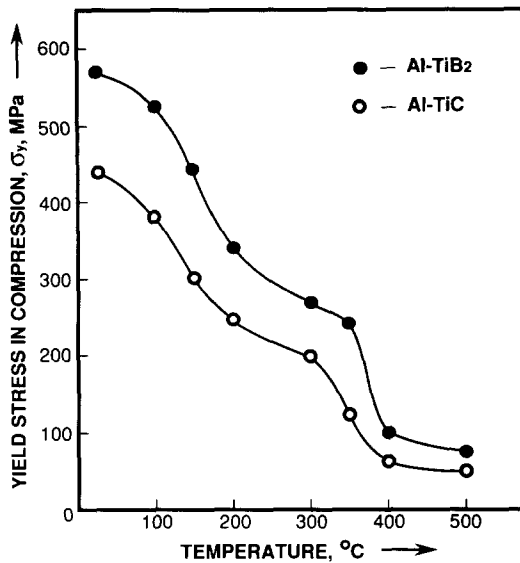
Fig. 12. Yield stress in compression of the cold-sintered ($P=$ 3 GPa, $T=300$ °C) SHS-processed TiC/Al and TiB$_2$/Al *in situ* composites as a function of temperature.

either on the basis of continuum mechanics models (*e.g.* shear lag, Eshelby and numerical models [40, 41]), or, alternatively, by considering modifications to the initial dislocation microstructure and including the effects of processing-induced residual stresses (*e.g.* incompatibiity–dislocation approach [42]). The continuum mechanics models are valid for MMCs reinforced with relatively large (at least several microns in size) particles [41] and predict only a very modest increase in σ_y with increasing volume fraction of reinforcement. It is apparent that these models cannot explain the high values of yield strength in the present work and therefore dislocation-related models should be addressed. The incompatibility–dislocation approach leads, for fine particles and spacing, to an Orowan-type relation of stress with both particle size and spacing [42]. For the approximately 0.1 μm size particles with an interparticle spacing of the same order of magnitude (Fig. 5(b)), the Orowan-type strengthening of Al will be $\Delta\sigma_y = 150$ MPa [24]. However, for the larger particle size and spacing (1–2 μm; Figs. 5(a), 6 and 7) the single-dislocation, Orowan-type hardening will be completely negligible. Nevertheless, these particles may contribute to the overall strengthening by another dislocation-related mechanism, namely the formation of dislocation tangles around particles resulting in a dislocation cell structure [42]. Similarly to Orowan-type hardening, the flow stress in this case is inversely proportional to the interparticle spacing. Unfortunately, since no reference to the value of the proportionality constant was given by the authors, no estimations of the relative importance of this mecha-

nism could be made in the present work. In addition, considering the fine microstructure of the composites obtained (Fig. 11), grain boundary strengthening may also be operative in these systems. We therefore assume that a superposition of the above dislocation-related strengthening mechanisms accounts for the high values of the yield stress of the SHS-processed *in situ* TiC/Al and TiB$_2$/Al composites. It should be mentioned that the fine microstructure obtained in these composites seems to be very stable: no decrease in the room temperature yield stress of TiC/Al and TiB$_2$/Al specimens was observed after annealing at 500 °C for 10 h (compare with rapidly solidified Al-base alloys, where coarsening of the fine intermetallic phases accompanied by a corresponding decrease in σ_y and σ_{UTS} is observed already at 350 °C [43]). The presence of the coarser (1–2 μm) hard TiC or TiB$_2$ particles should also result in a higher wear resistance. Preliminary pin-on-disc wear resistance tests have demonstrated a much better performance of SHS-processed Al-base composites compared with rapidly solidified Al-base alloys having otherwise similar room temperature mechanical properties [44].

It should be mentioned that, in spite of the high volume fractions of ceramic particles, the SHS-processed TiC/Al and TiB$_2$/Al composites exhibited pronounced ductility in compression: plastic strains ε_p, of 10%–15% (at room temperature) up to more than 25% (at elevated temperatures) were measured for both compositions. (Usually the room temperature plasticity in compression of Al matrix composites reinforced with 20–30 vol.% hard particles does not exceed about 4% [42, 45].) In three-point bending tests, too, a certain plastic deformation of the above materials was registered prior to the failure. The high levels of elevated temperature ductility observed in the SHS-processed Al matrix composites provide the possibility for more conventional (compared with cold sintering) densification routes, *e.g.* hot extrusion or forging. Thus, during high pressure consolidation at 300 °C, small amounts of TiC/Al and TiB$_2$/Al materials were extruded in a gap between the die wall and the punch, forming dense foils about 0.1 mm thick and about 5–6 mm long, indicating reasonable levels of composite ductility.

4. Conclusions

In the present research, Al matrix *in situ* composites with 30 vol.% of hard ceramic particles (TiC and/or TiB$_2$) were successfully fabricated by employing the SHS technique. This is the first study to report the SHS processing of Al-base MMCs with such a low volume fraction of the ceramic reinforcement. The result is significant and denotes that, by employing SHS, it is

possible to obtain Al matrix *in situ* composites with compositions ranging from 30 to 100 vol.% TiC and/or TiB$_2$ particles.

Using the SHS-processing route, very-fine-scale ceramic reinforcements ranging from tens of nanometers up to 1–2 μm were obtained in the Al matrix. The microscale TiC and TiB$_2$ particles were formed by the surface reaction between Ti dissolved in the Al melt and carbon or boron powder particles. A certain amount of unreacted carbon remained in the SHS-processed samples, presumably as a result of carbon black powder agglomeration. We believe that full conversion of carbon, as well as a more homogeneous microstructure of the SHS-processed materials, may be achieved if attrition milling is employed for the blending and refining of the starting powders. The mechanism of formation of the nanoscale TiC and TiB$_2$ precipitates remains to be elucidated but may be postulated to involve solution and reprecipitation.

It was shown that, by employing high pressure consolidation at temperatures not exceeding 300 °C, full density can be achieved in the porous SHS-processed Al matrix composites containing 30% TiC and/or TiB$_2$ particles. According to ref. 25, this consolidation route should also be feasible for SHS-processed Al-base MMCs with much higher volume fractions (up to 80 vol.%) of hard ceramic particles.

High room and elevated temperature mechanical properties (yield stress, microhardness) were obtained in the high-pressure-consolidated SHS-processed composites, comparable with the best rapidly solidified Al-base alloys with the same volume fraction (about 30%) of the second phase. These high properties were attributed to a superposition of Orowan-type hardening due to the high density of nanoscale ceramic particles, strengthening by formation of dislocation tangles around micron sized particles, and submicron grain boundary hardening. According to the preliminary results, SHS-processed Al matrix MMCs exhibit a wear resistance superior to that of rapidly solidified Al-base alloys with similar room temperature mechanical properties, apparently owing to the presence in the former of the dispersion of microscale hard ceramic particles.

Along with the high yield strength, appreciable room and elevated temperature ductility was observed in the SHS-processed Al-base composites. The high levels of elevated temperature ductility provide the possibility for these materials to be consolidated and shaped by the conventional hot-processing methods, *i.e.* hot pressing, extrusion and forging. It was observed that at temperatures up to at least 500 °C no coarsening of the microstructure occurred in the materials obtained. In order to better utilize the heat released during exothermic SHS reactions, the application of pressure

shortly after the passage of the combustion wave, while the sample is still at a relatively high temperature, may be attempted. Thus cemented carbide alloys prepared by the application of pressure after the passage of the combustion wave were reported to be fully dense [20]. This approach may be further developed into the concept of a continuous manufacturing process where the synthesized material is continuously densified immediately after the passage of the combustion wave at a rate equal to the combustion velocity. Al matrix *in situ* composites, with their low SHS combustion velocities (due to the strong heat dissipation in the "inert" metal matrix), as well as MMCs as a whole, may be an ideal choice for utilization of the continuous manufacturing process approach.

Acknowledgments

References

1 W. G. J. Bunk, *Mater. Sci. Eng. A, 134* (1991) 1087.
2 G. J. Hildeman and M. J. Koczak, *Treatise on Materials Science and Technology*, Vol. 31, Academic, New York, 1989, p. 323.
3 C. M. Adam and R. E. Lewis, in S. K. Das, B. H. Kear and C. M. Adam (eds.), *Rapidly Solidified Alloys*, TMS-AIME, Warrendale, PA, 1985, p. 157.
4 T. E. Tietz and I. G. Palmer, in G. Y. Chin (ed.), *Advances in Powder Technology*, ASM, Metals Park, OH, 1982, p. 189.
5 E. A. Starke, in R. C. Gifkins (ed.), *Strength of Metals and Alloys, Proc. ICSMA-6*, Pergamon, New York, 1982, p. 1025.
6 M. J. Koczak, S. C. Khatri, J. E. Alisson and M. G. Bader, in S. Suresh, A. Mortensen and A. Needleman (eds.), *Fundamentals of Metal Matrix Composites*, Butterworth-Heinemann, New York, 1993.
7 M. G. McKimpson and T. E. Scott, *Mater. Sci. Eng. A, 107* (1989) 93.
8 A. P. Divecha, S. G. Fishman and S. D. Karmerker, *J. Met., 33* (1981) 12.
9 C. G. Levi, C. J. Abbaschian and R. Mehrabian, *Metall. Trans. A, 9* (1978) 697.
10 A. P. Divecha and S. G. Fishman, in K. J. Miller and R. F. Smith (eds.), *Proc. 3rd Int. Conf. on Mechanical Behavior of Materials*, Pergamon, New York, 1980, p. 351.
11 P. Niskanen and W. R. Mohn, *Adv. Mater. Process., 133* (1988) 39.
12 A. R. C. Westwood, *Metall. Trans. A, 19* (1988) 749.
13 M. S. Newkirk, A. W. Urquhart, H. R. Zwicker and E. Breval, *J. Mater. Res., 1* (1986) 81.
14 M. J. Koczak and K. S. Kumar, In-situ process for producing a composite containing refractory material, *US Patent 4,808,372*, 1989.

15 S. Sampath, S. Khatri, E. Shtessel and M. J. Koczak, in V. A. Ravi and T. S. Srinvatsan (eds.), *Processing and Fabrication of Advanced Materials for High Temperature Applications II*, TMS, Warrendale, PA, 1993, p. 223.

16 A. K. Kuruvilla, K. S. Prasad, V. V. Bhanuprasad and Y. R. Mahajan, *Scr. Metall., 24* (1989) 873.

17 S. Khatri and M. J. Koczak, *Mater. Sci. Eng. A, 162* (1993) 153.

18 A. G. Merzhanov and I. P. Borovinskaya, *Dokl. Akad. Nauk SSSR, 204* (1972) 336.

19 A. G. Merzhanov and I. P. Borovinskaya, *Combust. Sci. Technol., 10* (1975) 195.

20 Z. A. Munir, *Ceram. Bull., 67* (1988) 342.

21 J. Subrahmanyam and M. Vijayakumar, *J. Mater. Sci., 27* (1992) 6249.

22 E. Y. Gutmanas, A. Rabinkin and M. Roitberg, *Scr. Metall., 13* (1979) 11.

23 E. Y. Gutmanas, *Powder Metall. Int., 15* (1983) 129.

24 E. Y. Gutmanas, *Prog. Mater. Sci., 34* (1990) 261.

25 E. Y. Gutmanas, in E. Arzt and L. Schultz (eds.), *New Materials by Mechanical Alloying Techniques*, DGM Informationgesellschaft, Oberursel, 1989, p. 129.

26 S. D. Dunmead, D. W. Readey, C. E. Semler and J. B. Holt, *Rep. UCRL-98773*, 1988 (Lawrence Livermore National Laboratory).

27 J. B. Holt, *Rep. UCRL-53258*, 1982 (Lawrence Livermore National Laboratory).

28 Y. Miyamoto, K. Hirao and M. Koizumi, *Proc. Int. Symp. on Fundamental Research Strategy in Development of New Materials for Efficient Energy Conversion, Osaka, 1987.*

29 A. N. Tabachenko, T. A. Panteleeva and V. I. Itin, *Combust. Explos. Shock Waves USSR, 20* (1984) 387.

30 Y. Choi, M. E. Mullins, K. Wijayatilleke and J. K. Lee, *Metall. Trans. A, 23* (1992) 2387.

31 O. Botstein, E. Y. Gutmanas and A. Lawley, in *Progress in Powder Metallurgy*, Vol. 41, MPIF, Princeton, NJ, 1986, p. 123.

32 J. C. Schuster, H. Nowotny and C. Vaccaro, *J. Solid State Chem., 32* (1980) 213.

33 A. Jarfors, H. Fredriksson and L. Froyen, *Mater. Sci. Eng. A, 135* (1991) 119.

34 M. Hansen, *Constitution of Binary Alloys*, McGraw-Hill, New York, 1958.

35 R. C. Dorward, in A. V. Clack (ed.), *Light Metals*, Vol. 1, TMS-AIME, New York, 973, p. 105.

36 C. J. Simensen, *Metall. Trans. A, 20* (1989) 191.

37 A. Banerji and W. Reif, *Metall. Trans. A, 17* (1986) 2127.

38 H. Yokokawa, N. Sakai, T. Kawada and M. Dokiya, *Metall. Trans. A, 22* (1991) 3075.

39 S. Ezz, M. J. Koczak, A. Lawley and M. K. Premkumar, in G. J. Hildeman and M. J. Koczak (eds.), *High Strength Powder Metallurgy Aluminum Alloys II*, TMS-AIME, Warrendale, PA, 1986, p. 287.

40 J. M. Papazian and P. N. Adler, *Metall. Trans. A, 21* (1991) 401.

41 G. Bao, J. W. Hutchinson and R. M. McMeeking, *Acta Metall. Mater., 39* (1991) 1871.

42 S. V. Kamat, J. P. Hirth and R. Mehrabian, *Acta Metall., 37* (1989) 2395.

43 O. Botstein, E. Y. Gutmanas and A. Lawley, in *Modern Developments in Powder Metallurgy*, Vol. 39, MPIF, Princeton, NJ, 1985, p. 761.

44 E. Y. Gutmanas, personal communication, 1993.

45 J. Yang, S. M. Pickard, C. Cady, A. Evans and R. Mehrabian, *Acta Metall. Mater., 39* (1991) 1863.